Effects of Electrolyte Flushing and Surface State on Electropolishing TB2 Titanium Alloy

Ying Wei
Nanjing University of Aeronautics and Astronautics
Xiaolong Fang (xlfang@nuaa.edu.cn)
Nanjing University of Aeronautics and Astronautics
Ningsong Qu
Nanjing University of Aeronautics and Astronautics
Di Zhu
Nanjing University of Aeronautics and Astronautics

Research Article

Keywords: Surface integrity, electropolishing, surface pretreatment, titanium alloy.

Posted Date: November 10th, 2021

DOI: https://doi.org/10.21203/rs.3.rs-1049118/v1

Version of Record: A version of this preprint was published at The International Journal of Advanced Manufacturing Technology on January 28th, 2022. See the published version at https://doi.org/10.1007/s00170-022-08754-8.

Abstract

TB2 titanium alloys are widely used in the aerospace industry. A high surface quality is required for the performance and fatigue life of titanium alloy parts. Electropolishing is useful for thin metal plates owing to its good processability and conformability. In this study, electrolyte flushing was proposed for electropolishing a large surface and a NaCl-containing ethylene glycol electrolyte was adopted. Three different mechanical grindings were employed for pretreatment, and the ideal surface quality was obtained with a rubber grinding head. Therefore, in the process of electropolishing a large surface, electrolyte flushing is superior to stirring because its flow field is even and controllable. The effects of the main processing parameters (voltage, flow rate, and process time) on the surface roughness and morphology were studied. Finally, a mirror-like surface with a surface roughness of 10.5 nm was obtained after flushing electropolishing for 30 min under a voltage of 25 V and a flow rate of 0.84 m/s.

1 Introduction

TB2 titanium alloy is a typical near-β titanium alloy. It has high specific strength, toughness, and elasticity. Sheet parts are commonly used for the skin of aircraft missiles and satellite-connecting belts. TB2 is highly sensitive to various surface defects, such as microcracks and scratches, which significantly affect the fatigue life of parts [1–3]. Surface defects affect both the high-cycle fatigue life and low-cycle fatigue life, whereas the surface roughness affects the high-cycle fatigue life [4–6]. Polishing is a common method for improving the surface integrity and fatigue life of titanium alloy parts. Shahzad et al. found that the surface morphology plays a key role in the initiation of fatigue cracks, accounting for 90% of the fatigue life [7, 8]. Novovic et al. [9] found that without considering the residual stress, when the surface roughness Ra > 0.1 μm, the surface morphology has an effect on fatigue. When the surface roughness Ra < 0.1 μm, the surface morphology has no effect on fatigue. Owing to the high hardness and low thermal conductivity of TB2 titanium alloy, significant grain wear and surface burns can occur during grinding [10]. A common surface treatment is manual grinding, which causes dust pollution, and is labor-intensive. Because of its good processability and consistency, electrochemical machining is suitable for polishing parts with complex shapes, slender parts, and thin plates, as it has good reproducibility [11–13].

The electropolished surface quality is affected by the electrolyte flow status and the dissolution state of different materials [14]. Because most of the materials are multiphase, the formation of the surface during electropolishing is affected by different mechanisms. Yi et al. [15] found that when the volume ratio of the electrolyte is 1 : 10 (H_2SO_4 : CH_3OH), the etching is isotropic. This electrolyte can be used for general metal polishing. In addition, these authors found that the surface roughness of TA2 decreases sharply from 64.1 nm to 1.2 nm. When electropolishing a titanium alloy, the type of electrolyte can fundamentally change the pitting characteristics and surface morphology during the entire electrochemical machining process [16–18]. Moreover, an environment-friendly electrolyte should be considered [19].

An ethylene glycol-based electrolyte is especially conducive to the formation of a polishing film owing to its high viscosity. It can produce a bright and pit-free finish [20]. Fushimi and Habazaki [21] studied the dissolution behaviour of pure titanium in NaCl-containing ethylene glycol. They found that the mass transfer is controlled by titanium species, such as the $TiCl_4$ adhesive layer. Kim et al. [22] further studied the effect of the surface adhesive layer on surface dissolution. They added 20% ethanol in a 1 mol/L NaCl-containing ethylene glycol solution to regulate the $TiCl_4$ adhesive layer, and then obtained a surface with Ra = 2.341 nm on pure titanium. Ferreri et al. [23] used an ethanol-ethylene glycol-NaCl electrolyte to prepare the EBSD samples, and collected high-quality EBSD datasets. Moreover, Huang et al. [24] placed the anode in translational motion to control the surface adhesive layer, obtaining a surface roughness Ra of 1.9 nm on a Ti-6Al-4V alloy surface. NaCl-containing ethylene glycol is an environment-friendly electrolyte with a good polishing surface quality and simple equipment, which has a promising future in production. However, the majority of previous research has been conducted in a beaker with a small sample size, and the mechanical stirring and translational motion are not adequate for polishing a large surface.

In addition, because the surface oxide layer hinders the anodic dissolution in the electropolishing process, most researchers have used sandpaper for mechanical polishing to improve the surface reactivity in the pre-treatment stage. [21–23, 25] However, different surface treatment processes affect the surface roughness, microstructure, and stress state of the materials, which can change their sensitivity to corrosion [26]. Zuo et al. [27] noted that the nucleation rate of metastable pitting increases with an increase in the surface roughness of polished stainless steel. Furthermore, appropriate surface treatment can also improve the fatigue life of the surfaces. [28, 29] Lopez-Ruiz et al. [30] found that the surface obtained by conventional shot peening as a pre-treatment is smoother than that obtained by severe shot peening, because the severe shot peening produces obvious dimples and surface defects. Therefore, to find the ideal pre-treatment method, it is necessary to study the influence of the surface state on the corrosion behaviour during electropolishing. The importance of surface pre-treatment has been neglected in previous studies using NaCl-containing ethylene glycol.

In this study, mechanical grinding was used to remove the thick oxide layer on the surface of TB2 titanium alloy sheets to improve the reactivity of electropolishing and remove large surface defects.[31] The effect of different surface states on electropolishing was studied through surface roughness, surface topography, and 3D profile. Thereafter, an appropriate grinding method was found. Therefore, to electropolish a large surface, flushing electropolishing was adopted to improve the inconsistent surface quality owing to stirring. This is because electrolyte flushing quickly refreshes the electrolyte in the processing area and removes heat and reaction products. The flow field is even and controllable. A good surface quality was obtained under the optimised parameters, which verifies the possibility of large surface polishing in the flushing electrolyte.

2 Materials And Methods

2.1 Preparation

The sample used in this study composed of forged TB2 titanium alloy (Ti-5Mo-5V-8Cr-3Al). Its surface was initially covered with a thick oxide layer (approximately 10 μm). The sample was cut into 20 × 10 mm and 40 × 20 mm plates using wire electrical discharge machining. As shown in Fig. 1, three different grinding heads were used to roughly remove the black oxide layer, producing three different surface finishes for electropolishing. A rubber grinding head is normally elastic, thus ensuring the uniformity of the grinding trace as well as reducing surface roughness. The grinding scratches were shallow. A feltless head was used with polishing paste for buffing, and the surface became more smooth. Therefore, the amount of material removed by the feltless buffing was significantly less than that of the other methods. The surface was pretreated with a feltless head until a metallic lustre was observed. Green carbon wheels are commonly used for grinding titanium alloys. In this experiment, we used a 1500 grit abrasive. In this process, the material removal should reach 20 μm when pretreated by a rubber grinding head or a green carbon wheel. To remove the polishing paste and dust left on the surface, the samples were ultrasonicated in acetone, ethanol, and deionised water separately for 5 min, and then dried.

2.2 Electropolishing

The molar concentration of the NaCl-containing ethylene glycol electrolyte is 1 mol/L [21]. Electropolishing was performed at room temperature (20°C). According to Kim and Huang et al. [22, 24], the anode surface is covered with a $TiCl_4$ layer. This layer is a sticky yellow liquid, and controlling the dissolved tetravalent titanium species is a probable rate-determining step. The anodic reactions during electropolishing are as follows:

$$Ti = Ti^{4+} + 4e^- \quad (1)$$

$$Ti4^+ + 4H_2O \rightarrow Ti(OH)_4 + 4H^+ \quad (2)$$

$$Ti(OH)_4 \rightarrow TiO_2 + 2H_2O \quad (3)$$

$$Ti^{4+} + 4Cl^- \rightarrow TiCl_4 \quad (4)$$

Figure 2(a) shows the electropolishing apparatus. The electrolyte was stirred in a 1-L glass beaker. A special fixture was designed to hold the workpiece. The power supply was controlled using software, and the current was measured in real time. Because the rotational speed is a key factor for the surface viscosity layer, the rotation speed was varied from 150 to 300 rpm. The machining gap was 20 mm, and the polishing voltage was 20–35 V. Figure 2(b) shows the apparatus used for flushing electropolishing. The electrolyte flows from the electrolyte tank through the pump and flow controller, and is then ejected from the cuneate inlet. After a long cycle, the increase in temperature of the electrolyte owing to electropolishing and the heat from the pump was controlled by circulating cooling water. The electrolyte flow rate was controlled using a flow meter. The cross section of the cuneate inlet was a rectangle with a

length of 30 mm, width of 2 mm, and transition length of 15 mm. The distance between the workpiece and cathode was 25 mm, and they were symmetrically placed at the inlet. The workpiece was placed 50 mm from the inlet. Compared with stirring, the flow field during flushing was more uniform when processing larger workpieces.

2.3 Characterization and testing

After electropolishing, the sample was ultrasonicated with ethanol and deionised water for 5 min, and then dried. The sample was weighed with an electronic balance (AE240, Mettler Toledo, Switzerland) before and after electropolishing to calculate the thickness of the material removed. The surface roughness was measured using a Taylor roughness profilometer (Talysurf i-Series 5, Taylor Hobson, UK). Each parameter was tested repeatedly, and the surface of the workpiece was measured at three different areas to obtain an average value and reduce the experimental error. The surface morphology was observed using a scanning electron microscope (SEM; Sigma 04-60, Zeiss, Germany), digital microscope system (VHX 6000, Keyence, Japan), and atomic force microscopy (AFM; Dimension Edge AFM, Bruker, Germany).

3 Results And Discussion

3.1 Effects of mechanical pre-buffing on electropolishing with stirring

The surface morphologies of the samples ground using different tools are shown in Fig. 3. Surface roughness was determined using a Taylor roughness profilometer. The original surface roughness Ra ≈ 0.4 μm, and the surface roughnesses of (b) –(d) are 0.23, 0.29, and 0.33 μm, respectively. Mechanical scratches can be observed on the ground surface with a green carbon wheel. The surface pre-treated by the feltless polishing is smoother, but the original defects are retained. Rubber grinding produces a flat surface, and the mechanical scratches are shallow.

The samples were then electropolished by stirring in a beaker for 25 min. As shown in Fig. 4, the surface roughness of the polished sample can be as low as approximately 50 nm. For the three surfaces after the different pre-treatments, the surface roughness decreased with an increase in the rotation speed until the rotation speed reached 250 rpm. As shown in Figure 6, the material dissolution is not uniform at low speed, whereas at a high speed, there are large flow lines.

Figure 5 shows that for a rotation speed of 250 rpm, the minimum surface roughness can be obtained for a voltage of 30 V with a surface pre-treated with a rubber grinding head. The other two methods produced the lowest surface roughness at a higher voltage. The main reason for these differences may be that although the thick oxide film was removed by the rough pre-treatment, a translucent oxide film was produced because of the inevitable water in the solution. When and how the passive film ruptures depends on the surface morphology. As shown in Figure 7, round pits appear on the surface at lower current densities, and striped stripes appear at higher current densities.

Figure 8 shows SEM images of electropolished surfaces after pre-treatment with different tools and optimal parameters. The surface roughness Ra of (a)-(b) are 47.9 nm, 58.4 nm, and 87.1 nm. Compared with Fig. 3, the electropolished surface is affected by the initial rough polished surface. As indicated above, samples pre-treated by feltless buffing and green carbon grinding wheel has the lowest surface roughness at a higher voltage of 35 V. A higher voltage usually generates more joule heat, thus the temperature increases rapidly because of the low specific heat capacity of ethylene glycol. The viscosity of electrolyte decreases with an increase of the temperature, resulting in visible flow lines on the surface. Moreover, from repeated experiments, we found that the electropolished surface roughness quite changes after feltless buffing. Because the material removal rate of feltless buffing is low, the final surface quality is affected by the original surface.

3.2 Electrolyte flushing to electropolishing large surface

According to the discussion in the previous section, the rubber grinding head was selected for surface pre-treatment in a later experiment. Figure 9 shows a surface polished by stirring in a beaker. The workpiece is larger (40 × 20 mm) instead of 20 × 10 mm. The electrolyte velocity varies over the surface. Correspondingly, the removal of reaction products and electrolytes occur at various rates, which result in different thicknesses of the adhesive layer of the $TiCl_4$ reaction product and different current densities. Defects appeared when the flow rate was low, and the reaction products accumulated, as shown in Figs. 9(a) and (c). The surface roughness Ra values of (a) and (c) are 113 nm and 45 nm, respectively. Thus, in our subsequent tests, a surface pre-treated by rubber grinding was electropolished for 30 min with lateral flushing.

Figure 10 shows AFM images of surfaces polished with flow rates at the inlet of 0.28 m/s, 0.56 m/s, 0.84 m/s, and 1.12 m/s. The surface roughness in (a) to (d) are 216 nm, 76 nm, 15.3 nm, and 29.3 nm. For a low flow rate, the reaction products were not discharged quickly, which affected the electrochemical polishing. With an increase of the flow rate, the surface roughness decreased rapidly. It was optimum when the flow rate at the inlet was 0.84 m/s. However, the surface deteriorated when the flow rate was significantly fast because there was an adhesive layer on the surface and the current density increased, as shown in Fig. 10(d). Figure 11 shows the morphologies of surfaces polished with different voltages at a flow rate of 0.84 m/s. The surface roughness in (a) to (c) are 33.7 nm, 10.6 nm, and 23.6 nm. Although the voltage has sight effect on the surface roughness, the minimum surface roughness is 10.6 nm when the voltage is 25 V. The surface roughness is more affected by the flow rate.

Figure 12 shows the current transients during the flushing electropolishing. The current density first decreases rapidly because there is no adhesive layer, and then changes slowly. Moreover, the current density increases with an increase in the flow rate or voltage. With an increase in the flow rate, the adhesive layer becomes too thin to maintain a stable processing current, as shown in Fig. 12(a). At a high voltage, the temperature of the processing zone increases sharply. It is well known that viscosity decreases with increasing temperature. As the viscosity decreases, the adhesion of the adhesive layer decreases, which destroys its dynamic balance, as shown in Fig. 12(b). Thus, an appropriate flow rate is an important factor for the surface quality. The dissolution of titanium in electropolishing with NaCl-

containing ethylene glycol electrolyte is controlled by the adhesive layer of the $TiCl_4$ reaction product; thus, maintaining the dynamic balance of the adhesive layer is the key factor in maintaining the ideal dissolution rate.

3.3 Relation between surface quality and material removal

Fig 13 shows the average current density vs. flow rate and cell voltage, corresponding constant voltage at 25 V, and constant flow rate at 0.84 m/s. It can be observed that the current density increases with an increase in the voltage and flow rate. Figure 14 shows that the material removal rate is linearly related to the current density. As discussed in the previous section, a surface with high quality and low surface roughness can be obtained when the voltage is 25 V and the flow rate is 0.84 m/s. Therefore, a surface with high quality and low surface roughness was obtained. Under these conditions, the generation and discharge of the adhesive layer are in a dynamic equilibrium. Moreover, the current density was stable, approximately 0.1 A/cm^2, and the corresponding material removal rate was approximately 1 μm/min.

The material removal rate and surface roughness over time are shown in Fig. 15. The surface roughness decreases rapidly in the first 10 min, and the material removal rate increases. Subsequently, the surface roughness decreases slowly. However, excessive polishing slightly increases the surface roughness. After 10 min, the material removal rate remains almost constant. Figure 16 presents 3D images of samples electropolished for different times, and the surface roughness values in (a) to (d) are 96.7 nm, 34 nm, 10.5 nm, and 14.8 nm. The sample treated for 30 min has the smoothest surface. The mirror effects of the surface and its surface topography are shown in Fig. 17. The surface roughness Ra is 10.5 nm, under the optimised parameters listed in Table 1.

Table 1
Optimized parameters for flushing electropolishing

Parameter	Value
Cell voltage (V)	25
Interelectrode gap (mm)	25
Flow rate (m/s)	0.84
Time (min)	30

4 Conclusions

In this study, an environment-friendly NaCl-containing ethylene glycol electrolyte was adopted for electropolishing thin plates composed of TB2 titanium alloy. The influence of different pre-treatments on the surface morphology after electropolishing was studied. The experimental processes in flushing

electropolishing were analysed, and the machining parameters were optimised. The following conclusions can be drawn:

(1) Mechanical buffing was applied to remove the thick oxidation layer formed on the forged plate during heat treatment. A rubber grinding head was selected for subsequent experiments because of its good surface consistency and quality after electropolishing. The surface roughness Ra was 47.9 nm.

(2) The experiments demonstrated that electrolyte flushing resulted in a more uniform flow field and produced a more even surface compared to stirring in a beaker.

(3) During flushing electropolishing, the adhesive layer was in dynamic equilibrium when the flow rate was 0.84 m/s and voltage was 25 V. The corresponding current density was approximately 0.1 A/cm^2, and the material removal rate was approximately 1 μm/min.

(4) For a flow rate of 0.84 m/s and a cell voltage of 25 V, a mirror-like surface with a surface roughness Ra of 10.5 nm was obtained after electropolishing for 30 min.

(5) The effects of pretreatment and flushing flow field on surface quality are discussed respectively. However, there are still some problems. a) A certain thickness of oxide layer formed in mechanical pretreatment, and the different crushing time in the initial stage of electrolysis affects the surface quality; b) Although NaCl-containing ethylene glycol electrolyte have good processability, the material removal rate is low. c) It is necessary to improve the flushing field for some common parts.

Declarations

Funding This project was supported by the National Natural Science Foundation of China (No. 91860208) and the Innovative Research Groups of the National Natural Science Foundation of China (No. 51921003).

Data availability All data generated or analyzed during this study are included in this published article.

Ethics approval Not applicable.

Consent to participate Not applicable.

Competing Interests The authors declare no competing interests.

References

1. Shahzad M, Chaussumier M, Chieragatti R (2010) Influence of surface treatments on fatigue life of Al 7010 alloy. J Mater Process Tech 210(13):1821–1826. https://doi.org/10.1016/j.jmatprotec.2010.06.019

2. Wang JL, Peng WJ, Yu J (2021) Effect of surface roughness on the fatigue failure and evaluation of TC17 titanium alloy. Mater Sci Tech-lond 37(6):1–13. https://doi.org/10.1080/02670836.2021.1885777
3. Su H, Shen X, Xu C (2020) Surface characteristics and corrosion behavior of TC11 titanium alloy strengthened by ultrasonic roller burnishing at room and medium temperature. J Mater Res Technol 9(4):8172–8185. https://doi.org/10.1016/j.jmrt.2020.05.059
4. Aigner R, Pusterhofer S, Pomberger S (2019) A probabilistic Kitagawa–Takahashi diagram for fatigue strength assessment of cast aluminium alloys. Mater Sci Eng 745:326–334. https://doi.org/10.1016/j.msea.2018.12.108
5. Cox A, Herbert S, Villain-Chastre JP (2019) The effect of machining and induced surface deformation on the fatigue performance of a high strength metastable β titanium alloy. Int J Fatigue 124(July):26–33. https://doi.org/10.1016/j.ijfatigue.2019.02.033
6. Herbert C, Axinte DA, Hardy M (2014) Influence of surface anomalies following hole making operations on the fatigue performance for a nickel-based superalloy. J Manuf Sci Eng 136:51016. https://doi.org/10.1115/1.4027619
7. Shahzad M, Chaussumier M, Chieragatti R (2010) Influence of surface treatments on fatigue life of Al 7010 alloy. J Mater Process Tech 210(13):1821–1826. https://doi.org/10.1016/j.jmatprotec.2010.06.019
8. Suraratchai M, Limido J, Mabru C (2008) Modelling the influence of machined surface roughness on the fatigue life of aluminium alloy. Int J Fatigue 30(12):2119–2126. https://doi.org/10.1016/j.ijfatigue.2008.06.003
9. Novovic D, Dewes RC, Aspinwall DK (2004) The effect of machined topography and integrity on fatigue life. Int J Mach 44(2–3):125–134. https://doi.org/10.1016/j.ijmachtools.2003.10.018
10. Xun LI, Chen Z, Chen W (2011) Suppression of surface burn in grinding of titanium alloy TC4 using a self-inhaling internal cooling wheel. Chin J Aeronaut 24(1):96–101. https://doi.org/10.1016/S1000-9361(11)60012-5
11. Trépanier C, Tabrizian M, Yahia L (1998) Effect of modification of oxide layer on NiTi stent corrosion resistance. J Biomedical Mater Res 43(4):433–440
12. Chen XL, Zhu JJ, Xu ZZ (2021) Modeling and experimental research on the evolution process of micro through-slit array generated with masked jet electrochemical machining. J Mater Process Tech 298:117304. https://doi.org/10.1016/j.jmatprotec.2021.117304
13. Wang D, Ren Z, Le H (2021) Improvement on the periodic dissolution behavior of titanium alloy in counter-rotating electrochemical machining. Int J Adv Manuf Tech. https://doi.org/10.1007/s00170-021-07235-8. 1-11
14. Wu M, Liu J, He J (2020) Fabrication of surface microstructures by mask electrolyte jet machining. Int J Mach 148:103471
15. Yi R, Zhang Y, Zhang X (2020) A generic approach of polishing metals via isotropic electrochemical etching. Int J Mach Tools Manuf 150:103517. https://doi.org/10.1016/j.ijmachtools.2020.103517

16. Sazou D, Saltidou K, Pagitsas M (2012) Understanding the effect of bromides on the stability of titanium oxide films based on a point defect model. Electrochim Acta 76:48–61. https://doi.org/10.1016/j.electacta.2012.04.158
17. Baehre D, Ernst A, Weisshaar K (2016) Electrochemical dissolution behavior of titanium and titanium-based alloys in different electrolytes. Procedia CIRP 42:137–142. https://doi.org/10.1016/j.procir.2016.02.208
18. Speidel A, Mitchell-Smith J, Bisterov I (2019) Oscillatory behaviour in the electrochemical jet processing of titanium. J Mater Process Technology 273:116264. https://doi.org/10.1016/j.jmatprotec.2019.116264
19. Vara GA, Butrón EJ, BelénGarcía-Blanco M (2015) Challenges and opportunities in next generation of electropolishing surfaces. Surf Eng 31(6):397–398
20. Liu W, Luo Z, Kunieda M (2020) Electrolyte jet machining of Ti1023 titanium alloy using NaCl ethylene glycol-based electrolyte. J Mater Process Technol 283:116731. https://doi.org/10.1016/j.jmatprotec.2020.116731
21. Fushimi K, Habazaki H (2008) Anodic dissolution of titanium in NaCl-containing ethylene glycol. Electrochim Acta 53(8):3371–3376. https://doi.org/10.1016/j.electacta.2007.11.074
22. Kim D, Son K, Sung D (2015) Effect of added ethanol in ethylene glycol–NaCl electrolyte on titanium electropolishing. Corros Sci 98(015):494–499. https://doi.org/10.1016/j.corsci.2015.05.057
23. Ferreri NC, Savage DJ, Knezevic M (2020) Non-acid, alcohol-based electropolishing enables high-quality electron backscatter diffraction characterization of titanium and its alloys: application to pure Ti and Ti-6Al-4V - sciencedirect. https://doi.org/10.1016/j.matchar.2020.110406. Mater Charact 166
24. Huang P, Lai J, Han L (2016) Electropolishing of titanium alloy under hydrodynamic mode. Sci Chin Chem 59(11):1525–1528. https://doi.org/10.1007/s11426-016-0211-y
25. Simka W, Socha RP, Dercz G (2013) Anodic oxidation of Ti–13Nb–13Zr alloy in silicate solutions. Appl Surf Sci 279:317–323. https://doi.org/10.1016/j.apsusc.2013.04.091
26. Li W, Li DY (2006) Influence of surface morphology on corrosion and electronic behavior. Acta Mater 54(2):445–452. https://doi.org/10.1016/j.actamat.2005.09.017
27. Zuo Y, Wang H, Xiong J (2002) The aspect ratio of surface grooves and metastable pitting of stainless steel. Corros Sci 44(1):25–35. https://doi.org/10.1016/S0010-938X(01)00039-7
28. Lago J, Guagliano M, Bokvka O (2017) Improvement of fatigue endurance of welded S355 J2 structural steel by severe shot peening. Surf Eng 33(9):1–6
29. Gao Y, Lu F, Yao M (2005) Influence of mechanical surface treatments on fatigue property of 30CrMnSiNi$_2$A steel. Surf Eng 21(4):325–328. https://doi.org/10.1179/174329405X40957
30. Lopez-Ruiz P, Garcia-Blanco MB, Vara G (2019) Obtaining tailored surface characteristics by combining shot peening and electropolishing on 316L stainless steel. Appl Surf Sci 492:1–7. https://doi.org/10.1016/j.apsusc.2019.06.042

31. Yang G, Wang B, Tawfiq K (2016) Electropolishing of surfaces: theory and applications. https://doi.org/10.1080/02670844.2016.1198452. Surf Eng 1-18

Figures

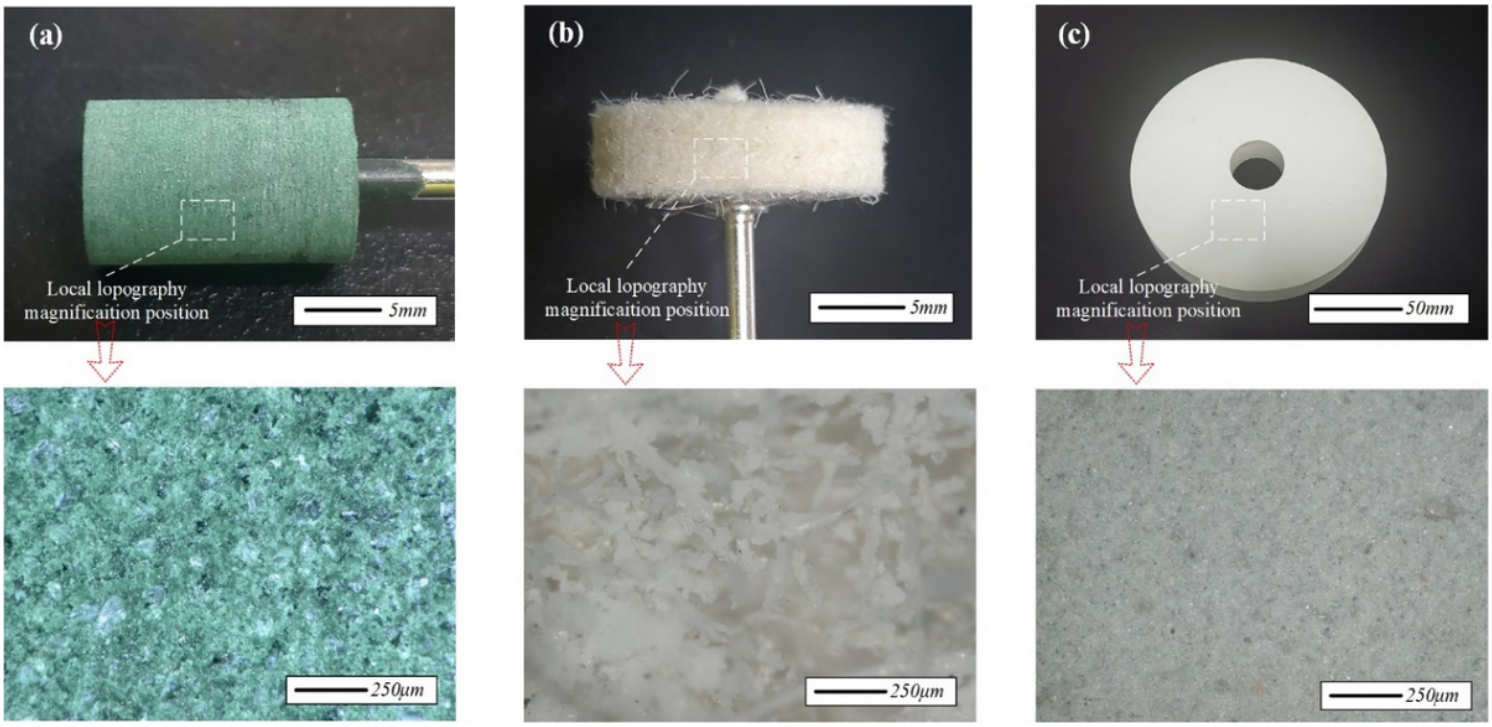

Figure 1

Three types of grinding heads and their surface topography: a rubber grinding head, b feltless buffing head with white polishing paste, and c green carbon grinding wheel

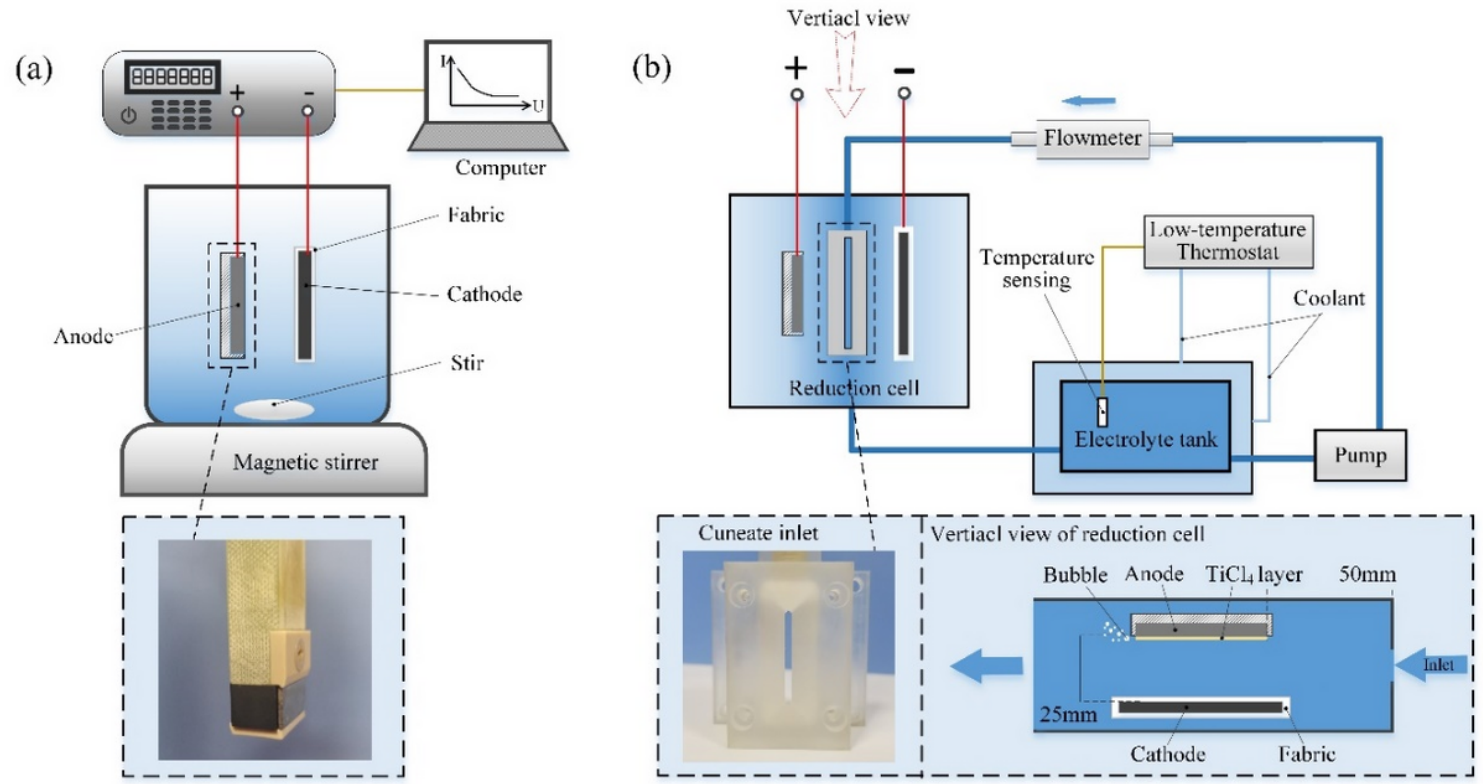

Figure 2

Two different electropolishing setups. a Electrochemical polishing in a beaker with stirring. b Flushing electropolishing

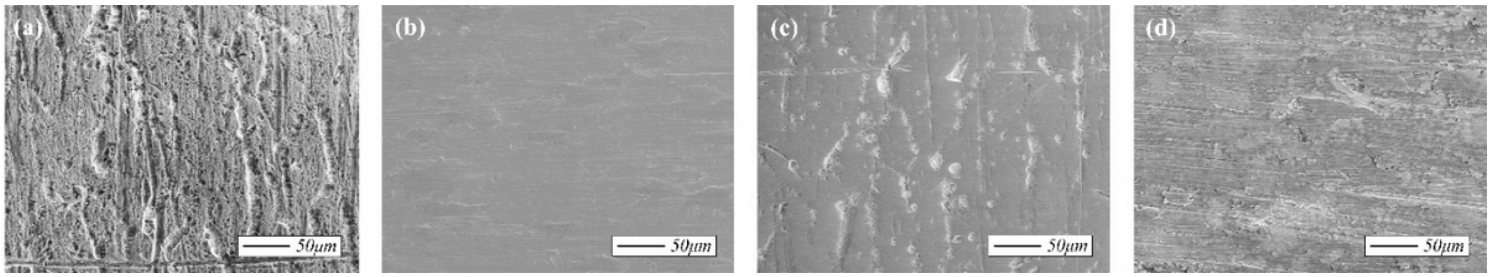

Figure 3

SEM images of a original surface and the surface pretreated by b a rubber grinding head, c feltless buffing, d a green carbon grinding wheel

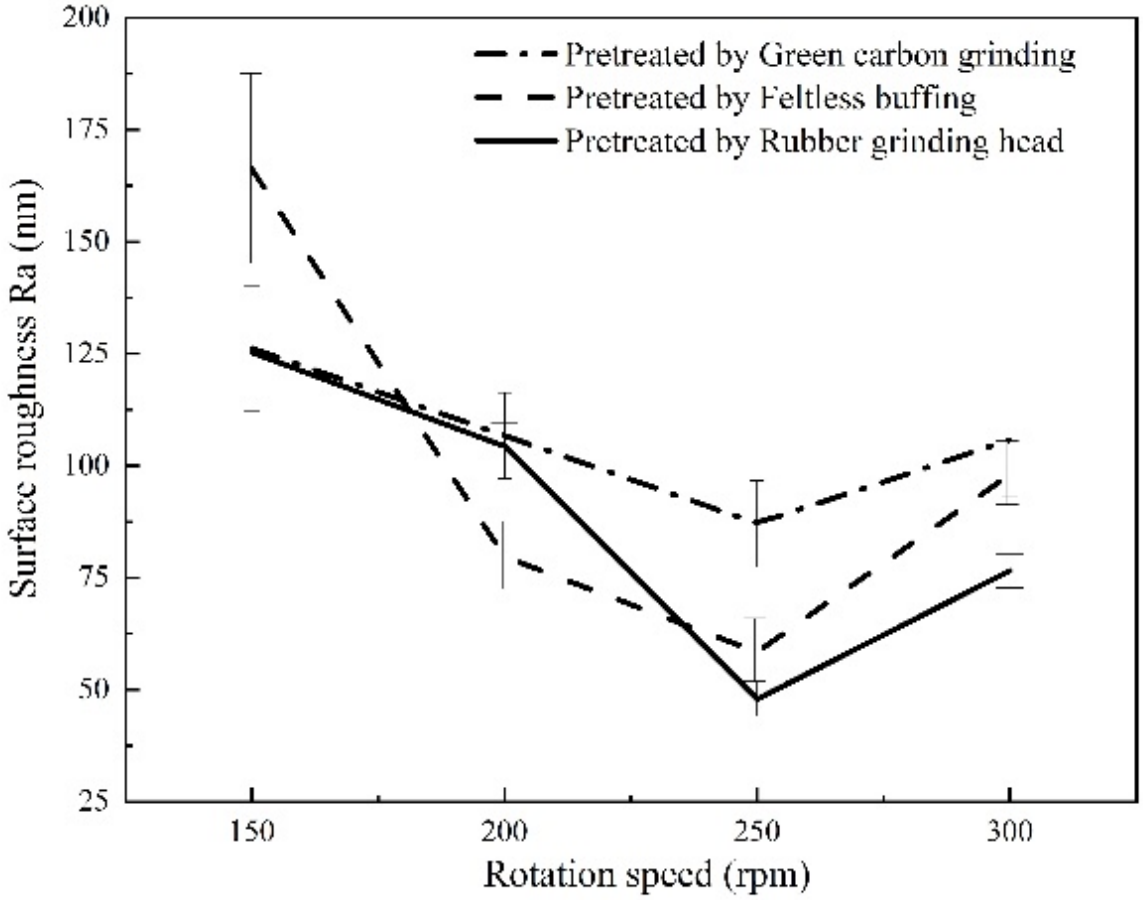

Figure 4

Electropolished surface roughness (Ra) vs. rotation speed at a constant voltage of 30

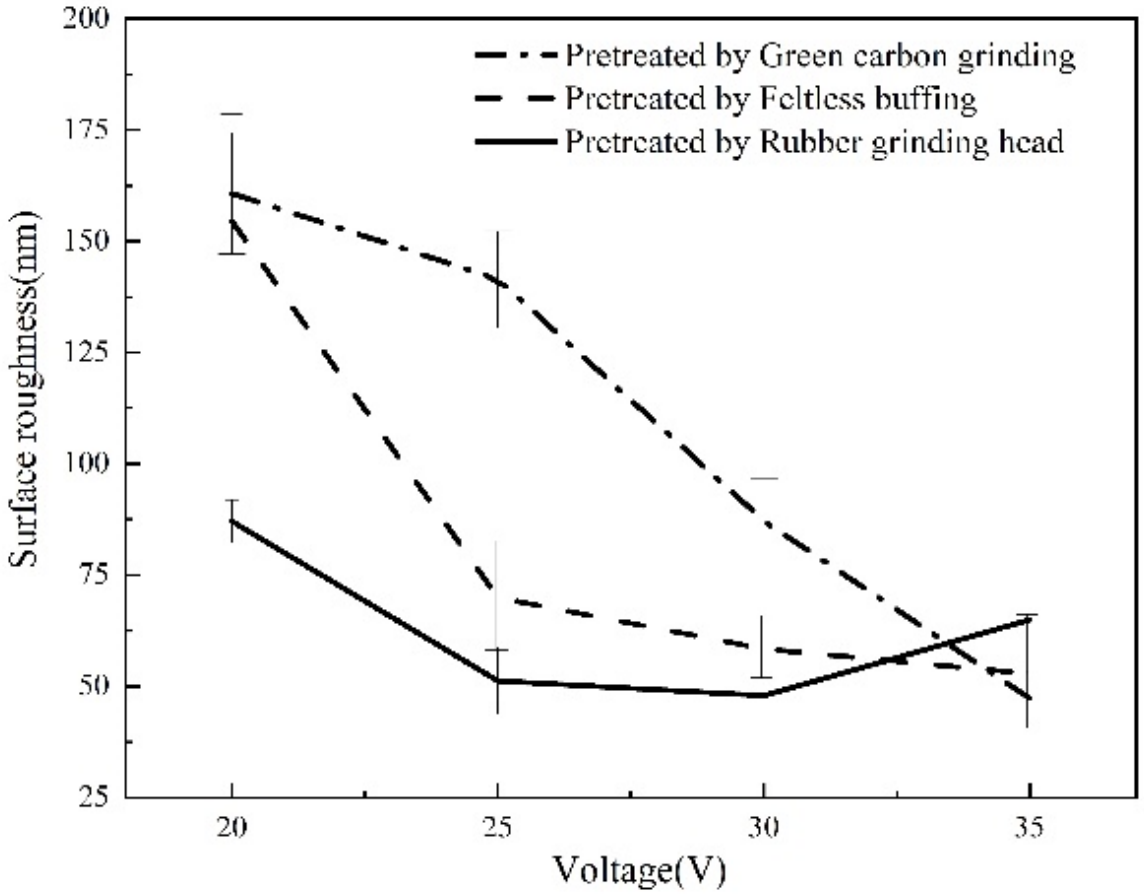

Figure 5

Electropolished surface roughness (Ra) vs. voltage at a constant rotation speed of 250

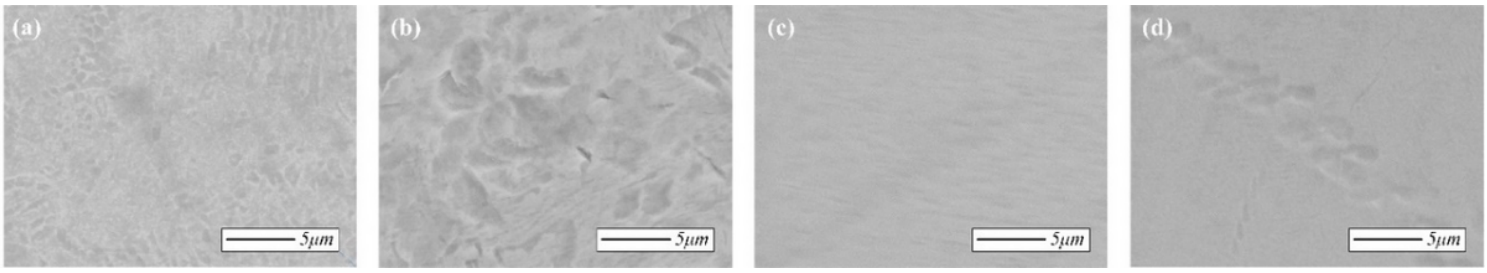

Figure 6

Surface topography of electropolished surface that pretreated with a rubber grinding head: a 150 rpm, b 200 rpm, c 250 rpm, and d 300 rpm

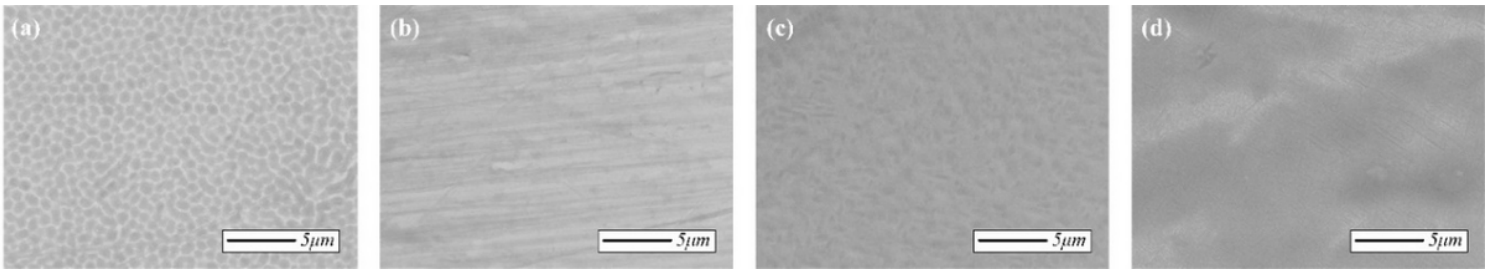

Figure 7

Surface topography of electropolished surface that pretreated with a rubber grinding head: a 20 V, b 25 V, c 30 V, and d 35 V

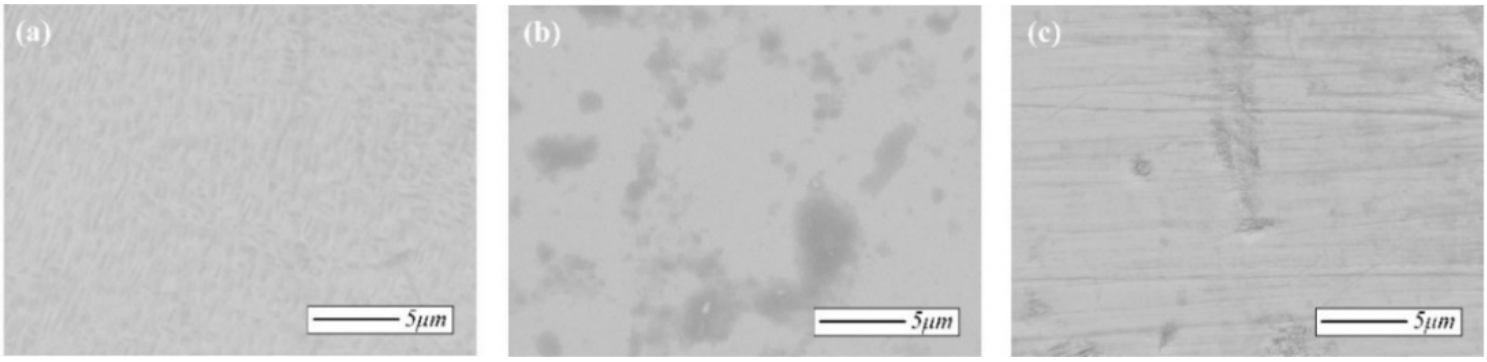

Figure 8

SEM images of surfaces electropolished under optimal parameters. a Pre-treated by a green carbon grinding wheel, and then electropolished at 35 V and 250 rpm for 30 min. b Pre-treated by feltless buffing, and then electropolished at 35 V and 250 rpm for 30 min. c Pre-treated by a rubber grinding head, and then electropolished at 30 V and 250 rpm for 30 min

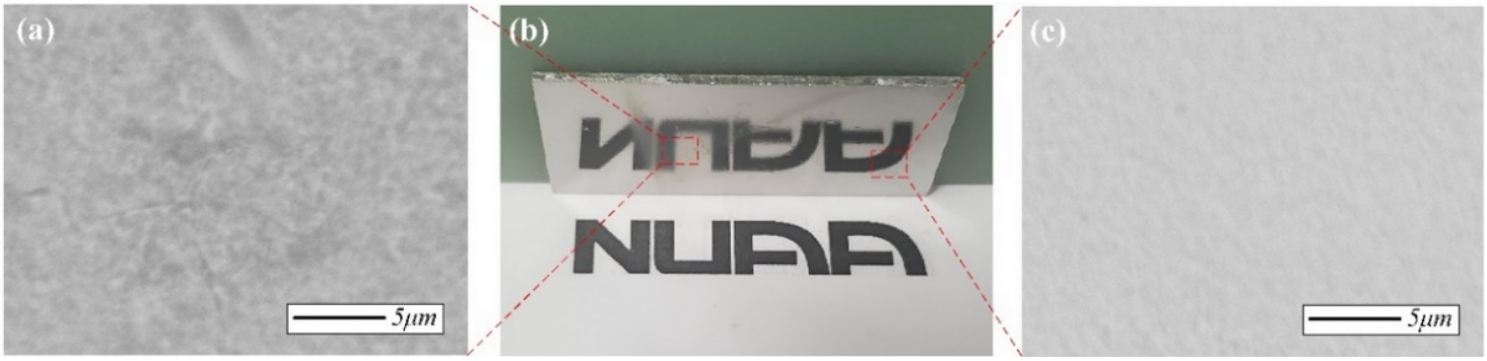

Figure 9

Surface of electropolished TB2 sheet with stirring in a beaker. a SEM image of surface defects, b whole sample, and c SEM image of a good part of the surface

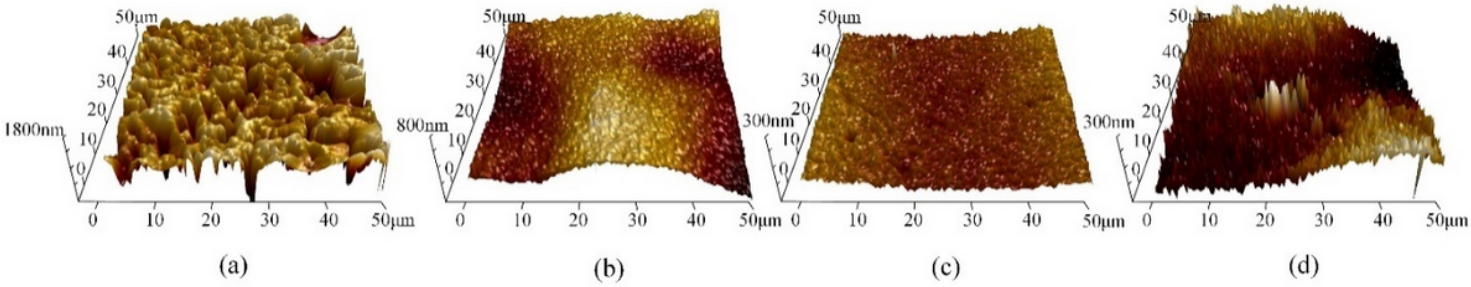

Figure 10

AFM images of surfaces after flushing electropolishing, the distance between the TB2 titanium alloy plates and the stainless steel plate is 25 mm

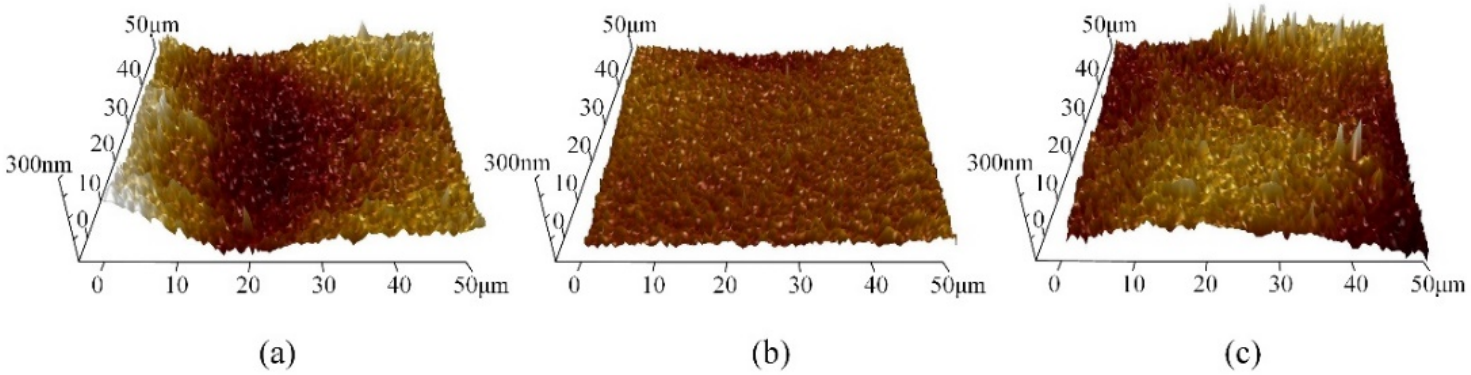

Figure 11

AFM images of surfaces after flushing electropolishing, and the flow rate is 0.84 m/s. The distance between the TB2 titanium alloy plates and the stainless steel plate is 25 mm

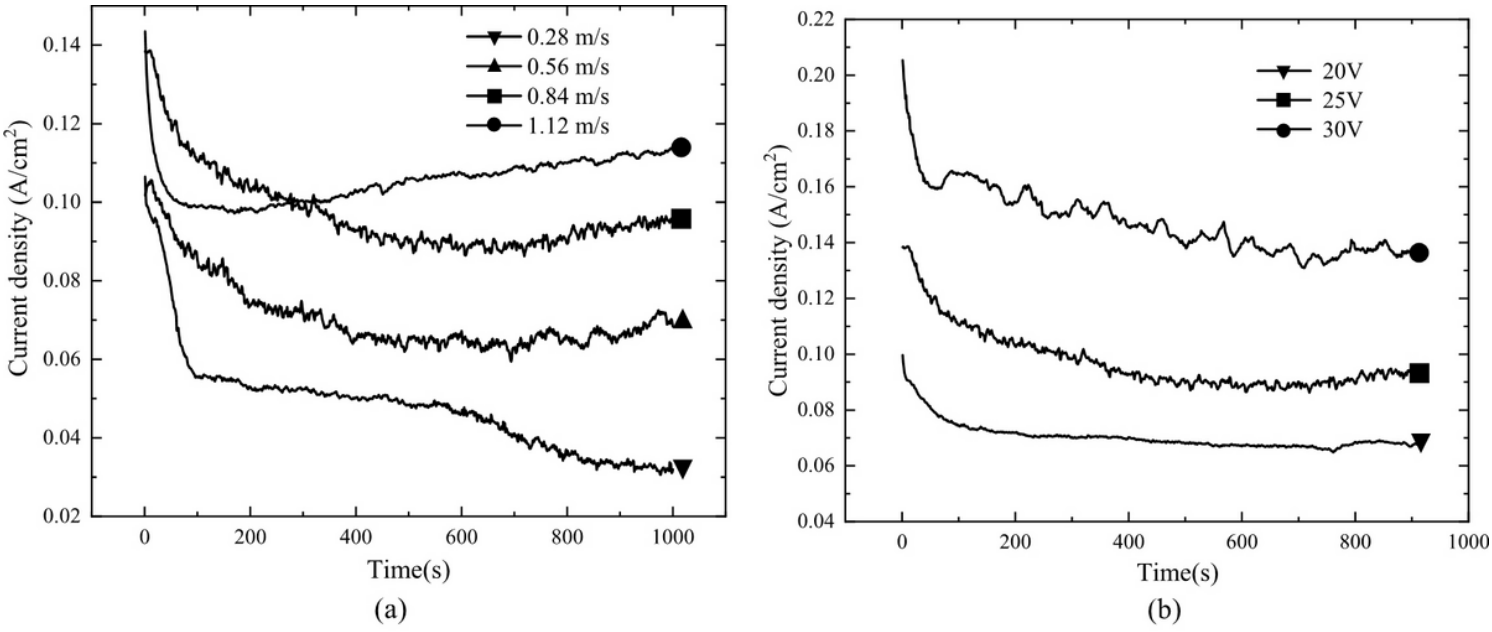

Figure 12

Current transients during flushing electropolishing over 1000 s. a) at different flow rates at 25 V and b at different voltages at 0.84 m/s

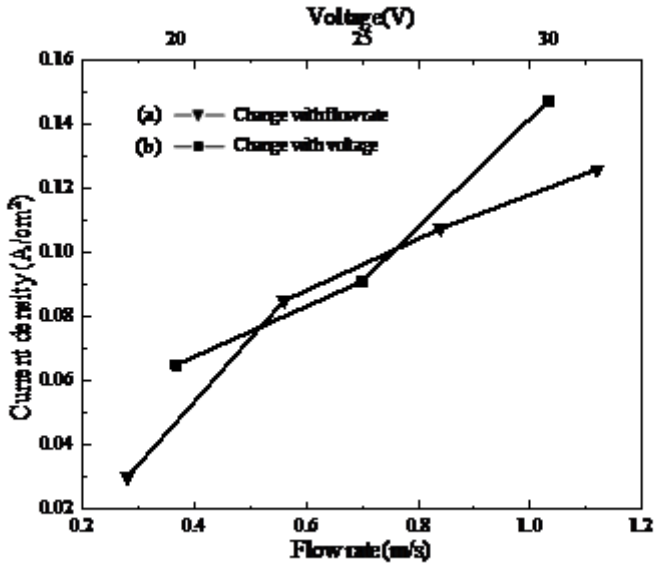

Figure 13

Average current density vs. flow rate and cell voltage

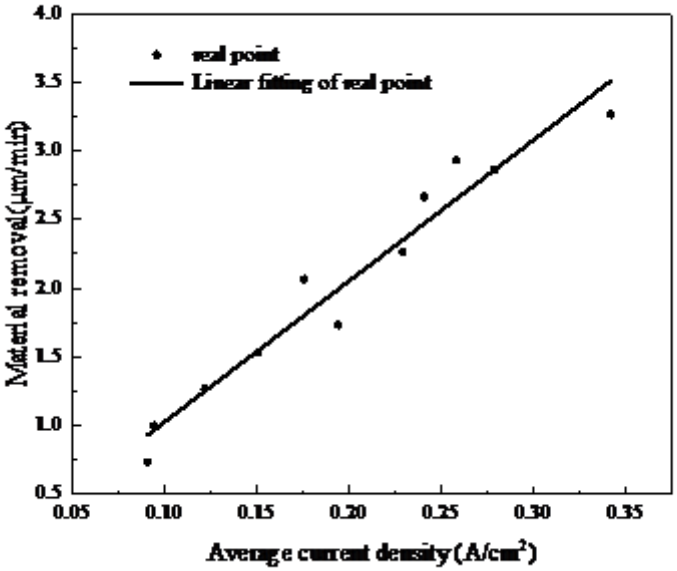

Figure 14

Material removal rate of electropoli-shing vs. average current density

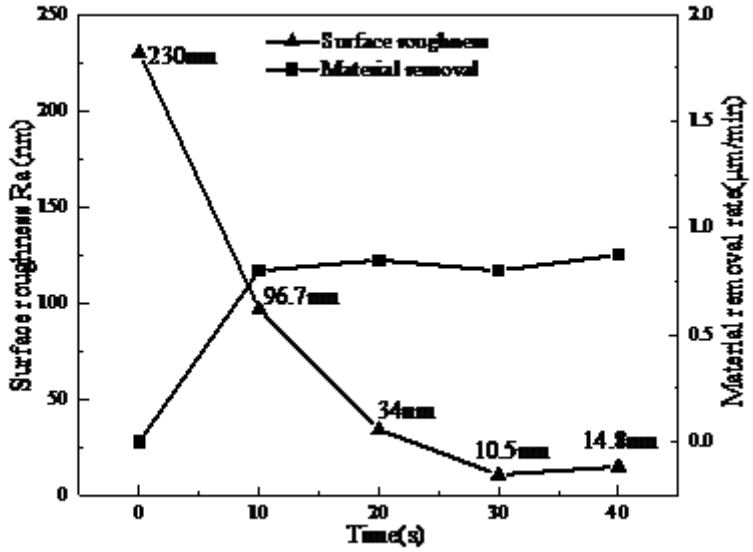

Figure 15

a Surface roughness (Ra) of an electropolished TB2 titanium alloy sample determined with AFM over time. b The material removal rate over time. The voltage was 25 V, and the flow rate was 0.84 m/s

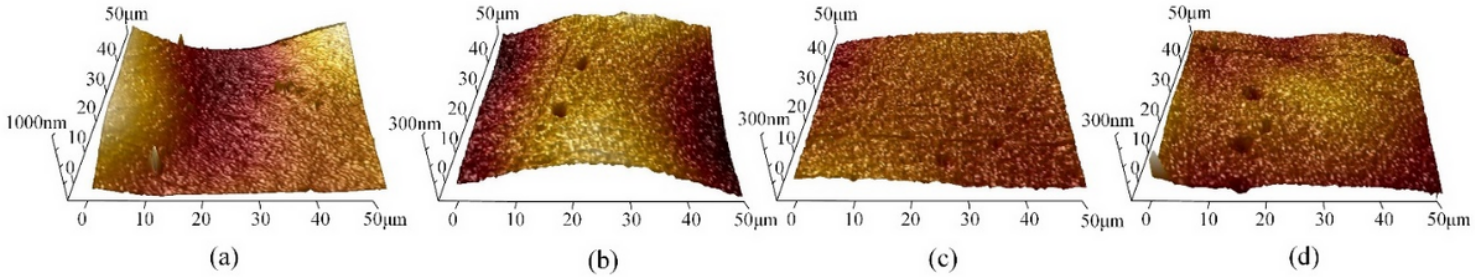

Figure 16

AFM images of TB2 samples electropolished for a 10 min, b 20 min, c 30 min and d 40 min

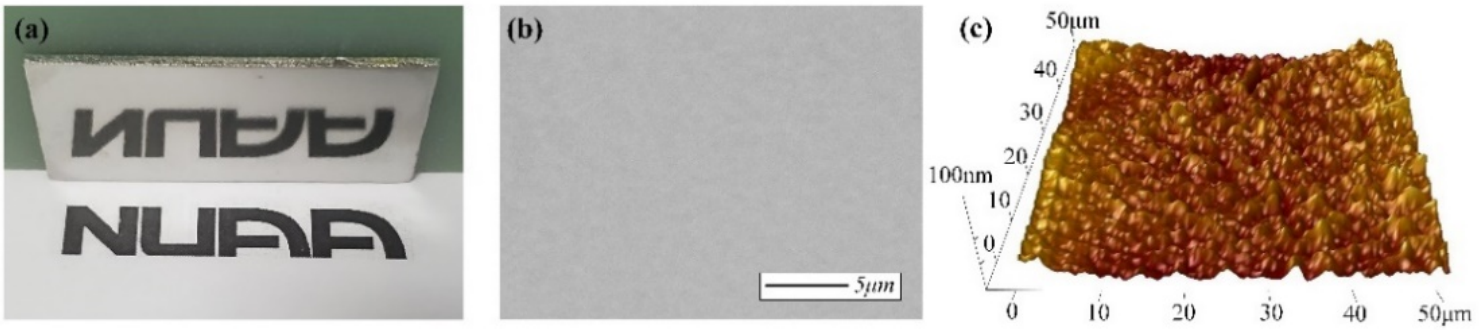

Figure 17

Electropolished TB2 sample: a Entire sample, b SEM image of surface morphology, and c 3D surface topography measured by AFM